

REVIEW OF PROPELLER-WING AERODYNAMIC INTERFERENCE

L.L.M. Veldhuis
Delft University of Technology

Keywords: *propeller-wing interaction, numerical modeling, experiments.*

Abstract

The main goal of this paper is to review the mechanisms and describe the phenomena that play a role in the aerodynamic interference between tractor propellers and a wing.

Moreover, the effect of various parameters like the propeller position and inclination will be discussed in detail. Besides this means to analyze propeller-wing design will be presented using calculation techniques of distinct complexity. Rather than an evaluation of the complete design envelope of a propeller powered concept, one typical aspect is investigated herein: the aerodynamic aspects of the propeller integration for the cruise phase of the aircraft.

Symbols

| | |
|-----------|---|
| a | axial inflow factor ($= v_a / U_\infty$) |
| a' | tangential velocity ratio ($= v_t / U_\infty$) |
| b | wing span |
| C_D | drag coefficient |
| C_L | lift coefficient |
| \bar{c} | mean aerodynamic chord |
| D | propeller diameter |
| G | propeller geometry influence function |
| I_w | Wing interference influence function |
| J | propeller advance ratio (U_∞ / nD) |
| P_c | power coefficient ($2\pi Q_c / J$) |
| Q_c | propeller torque coefficient |
| n | propeller speed |

| | |
|--------------------|---|
| R | propeller radius |
| Re | Reynolds number |
| T_c | thrust coefficient () |
| v_a | axial velocity increase |
| v_t | tangential velocity increase |
| x, y, z | coordinates in flow axis system |
| x_p, y_p, z_p | propeller position (centre of spinner) |
| α | angle of attack |
| α_p | propeller incidence angle relative to the wing reference line |
| $\alpha_{p_{eff}}$ | effective propeller angle of attack |
| $\beta_{0.75R}$ | propeller blade angle at $0.75R$ |
| η_p | propulsive efficiency |
| ω | propeller rotational speed |

Indices

| | |
|--------|--------------------|
| $corr$ | corrected |
| p | (due to) propeller |
| tot | total |
| w | (due to) wing |

1 Introduction

Modern aircraft concepts, like the European *A400M*, exhibit high disk loading and a high number of (swept) blades to enable high cruising speed. The strong swirl velocities in the slipstream combined with increased dynamic pressure generate a considerable deformation of the lift distribution, which has an impact on the aerodynamic behavior and performance of the wing. The wing loading in turn induces a disturbed inflow field for the propellers, especially in the case where the propeller and

the wing are closely coupled. Hence the aerodynamic interference for typical tractor propeller wing aircraft may be summarized as propeller effects on the wing and vice versa.

The description of the interactive flow around the propeller-wing configuration requires detailed information about the characteristics of the slipstream. Due to the self-induced velocities produced by the propeller vortex system the slipstream tends to deform and roll up which produces a so-called slipstream tube with strong gradients in various flow quantities both in streamwise and radial direction. In case of an asymmetrical loaded propeller, for example caused by a non-zero angle of attack of the thrust axis ($\alpha_{p_{eff}} \neq 0$), a variation of the flow quantities in azimuthal direction exists.

Summarizing one may state that the distribution of the axial velocity ratio, denoted with a , the tangential velocity ratio, denoted with a' , and the total pressure distribution, are a function of the propeller geometry (G_p), blade setting ($\beta_{0.75R}$), operating conditions (J), effective propeller angle of attack ($\alpha_{p_{eff}}$) and the (interference) effect of the wing on the flow around the propeller (I_w):

$$\begin{aligned} a(x_p, r) &= f_a(G_p, \beta_{0.75R}, J, \alpha_{p_{eff}}, I_w) \\ a'(x_p, r) &= f_i(G_p, \beta_{0.75R}, J, \alpha_{p_{eff}}, I_w) \\ p_t(x_p, r) &= f_p(G_p, \beta_{0.75R}, J, \alpha_{p_{eff}}, I_w) \end{aligned} \quad (1)$$

where the coordinates (x_p, r) are taken in the reference system fixed to the thrust axis. The fact that this thrust axis can have any position in space means that the relevant flow properties in the flow fixed reference system, (x, y, z) exhibit spatial distributions that without any form of symmetry.

For a selected cruise condition the parameter $G_p, \beta_{0.75R}$ and J are fixed. This means that the problem in the sense of the propeller wing interference is found in the dependency of $\alpha_{p_{eff}}$ and I_w on the propeller position relative to the wing and the aircraft state. A simple solution of

the problem is hindered by the fact that the latter parameters in turn are influenced by the form and position of the propeller slipstream. Hence the performance of the complete propeller-wing combination will only be attained by accepting a full interaction between propeller and wing which will be denoted as FIM (full interaction mode). Nevertheless many researchers have accepted the single interaction mode (SIM), in which the wing effect on the propeller is simply neglected. As will be shown in subsequent sections this SIM approach obstructs the analysis of the propeller position effects on the propulsive efficiency of the configuration.

Although the propeller exhibits a typical unsteady flow field it has been shown by several authors [1,2,3,4,5] that for most practical design calculations it is acceptable to treat the flow as being steady. This time-averaged approach will be adopted during the subsequent analysis of the propeller-wing interference problem.

2 Regions of influence

The slipstream properties change throughout the local flow field resulting in a strong deformation of the wing loading distribution. In this respect mainly the changes in radial direction and the streamwise development of the propeller slipstream must be taken into account. To describe the most important interference effect it is beneficial to split the wing and the propeller

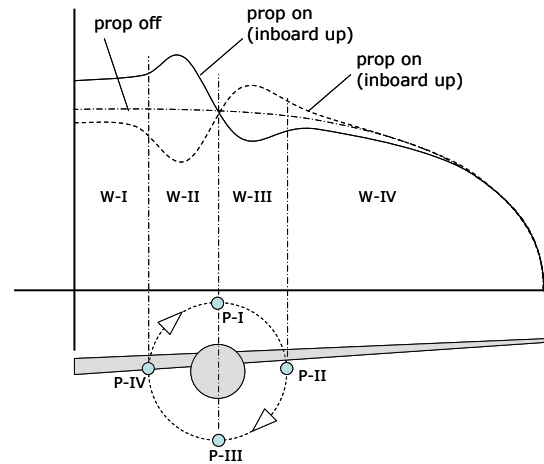


Fig. 1 Influence areas related to propeller-wing interaction based on the loading distributions.

in several regions of influence, as sketched in Fig. 1.

2.1 Wing regions

Wing regions, W-II and W-III are directly influenced by the slipstream that washes the wing. In W-II the lift effect of the propeller swirl velocity, that changes the local wing angle of attack, is enhanced by the increased dynamic pressure. Considering the IU rotation case, in W-III these two slipstream effects counteract each other. The result is a smaller difference between the powered and unpowered case in this region. It can be clearly seen that the propeller effect is not limited to the wing part (with a span equal to the contracted slipstream diameter) directly behind the propeller. Due to the changed wing inflow conditions generated by the propeller the loading in W-I and W-IV changes as well, both for the inboard and outboard up running propeller. This is the result of the distorted vorticity sheet that leaves the wing.

2.2 Propeller regions

To understand the wing effects on the propeller, 4 regions of influence can be defined (see Fig. 1). One should consider that these regions, located at azimuthal positions of $\theta = 0^\circ, 90^\circ, 180^\circ$ and 270° are in fact not completely “separated”. Rather, a gradual change of the slipstream properties is found going from one region to a neighboring one.

The effect of the presence of the nacelle is a small axial velocity increase in all four P-regions. As such the detailed nacelle effect on the propeller (which is quite small) is left out of the discussion on propeller-wing interference here.

Typical differences at P-II and P-IV are found due to the wing induced upwash. As sketched in Fig. 2 the local blade angle of attack increases at the downgoing blade side (P-II, for IU-rotating propeller) and decreases on the opposite side (P-IV). The result is a loading asymmetry in the slipstream that has to be accounted for in the propeller-wing interaction model.

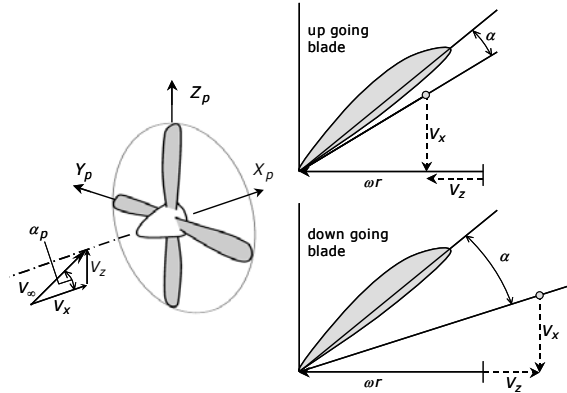


Fig. 2 Blade angle of attack variation due to propeller pitch angle.

The differences in the induced axial and tangential velocities found for P-I and P-III is attributed to the wing induced axial velocity increase and decrease for the high and low propeller blade position respectively.

3 Swirl recovery

An important facet in the calculation of the slipstream-induced velocities with simple models is the reduction of the rotational velocity in the slipstream due to the wing. Both experimental and numerical studies have shown that there is a significant reduction in rotation (swirl velocity) due to the presence of the wing. Various windtunnel tests have indicated that the amount of the reduction in the rotational velocity depends on numerous factors like the propeller position relative to the wing, the power setting, the wing loading and so forth.

It should be noted that while there is some reduction in rotational velocity due to friction and viscous effect, it is more likely that a change in the slipstream helix angle is the main cause for the reduction in the rotation in the rotational velocity. From a conceptual point of view the reduction in the slipstream helix angle can be attributed to the wing induced upwash (in front) and downwash (behind).

The wing is assumed to reduce the angle of rotation of the slipstream within those annuli that wash over it. In subsequent paragraph it will be shown that it is of vital importance to implement a Swirl Recovery Factor (SRF) in the simple static slipstream models to arrive at acceptable calculation results.

4 Analysis methods

The data presented in this paper were produced by CFD techniques of different complexity combined with a number of experiments. The main goal is to twofold: a) identify the influence of various flow parameters and configuration adaptations on the propeller-wing characteristics and the propulsive efficiency, b) determine to what level of complexity the prediction codes should be developed to acquire acceptable data that can be used in the preliminary design of propeller aircraft.

The numerical calculations that are described herein were performed at two levels:

- an enhanced vortex lattice code incorporating a Blade element Method (BEM)-analysis of the propeller
- a commercial Navier-Stokes code

The experiments were performed using three different windtunnel models:

- a straight wing-nacelle-propeller model, denoted PROWIM
- a straight wing model with separate (movable) propeller, denoted APROPOS
- a full 3D, 1:20 scale model of a typical turboprop aircraft (F27)

4.1 Prediction codes

4.1.1 VLM-BEM model

Although this method constitutes a rather crude model of the real flow around the wing its simplicity allows some interesting analyses to be performed. The reduced calculation time that is typical for the method allows a quick survey of various configuration layouts.

Adequate descriptions of the VLM technique can be found in open literature [6,7].

The effect of the propeller on the wing loading characteristics is based on the fact that at the control point position an additional velocity vector, V_p , induced by the propeller slipstream is introduced. The differences between earlier VLM-codes are typically found in the way these additional velocity components are calculated without compromising the original VLM-approach. In most cases, only a one-way interaction is implemented, e.g. only the propeller effect on the wing (further denoted as

single-interaction-mode or SIM) is modeled. The method suggested in this report employs a full interaction allowing the wing effect on the propeller as well (full-interaction-mode or FIM).

Adaptation of the undisturbed velocity contribution is required both on the lattice elements inside the slipstream tube and outside the slipstream tube since the local flow angles outside the slipstream are changed by the contraction (and deformation) of the slipstream. For the VLM models that were published up till now, however, this adaptation outside the slipstream tube was neglected. This leads to erroneous results when extreme positions of the propeller relative to the wing, like an over-the-wing arrangement are selected. The VLM-results described herein are based on the FIM approach taking into account the spatial development of the slipstream characteristics, including a swirl recovery factor SRF.

4.1.2 NS-model

The Navier-Stokes code that was used for the propeller-wing calculations is the commercial Fluent 6.1 package [8]. To model the propeller an actuator disk approach was adopted which prescribes the jump conditions at the propeller plane. Due to the asymmetry in the propeller loading the pressure and velocity are dependent both on the radial position and the azimuthal position of the cell faces that constitute the infinitesimal thin propeller plane [9,10].

4.2 Windtunnel models

4.2.1 PROWIM and APROPOS

The first wind tunnel model, denoted PROWIM (propeller wing interference model), consists of a straight wing of aspect ratio $A = 5.33$ with no twist, constant chord and airfoil section (NACA 64₂-A015). Its (half) span is 0.64 m . For the powered tests, the model is equipped with a 4-bladed metal propeller of 0.236 m diameter that is driven by a 5.5 kW electrical 3-phase induction motor contained inside the nacelle. The axis-symmetrical nacelle is mounted with its rotation axis on the MAC-line and at 0.3 m from the wing root. The dimensionless spanwise

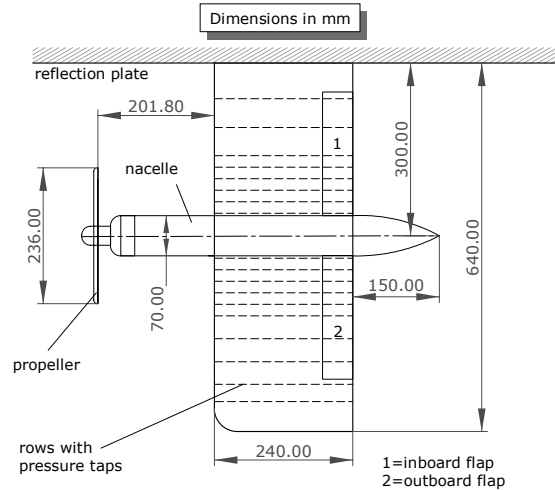


Fig. 4 Dimensions and layout of the PROWIM model.

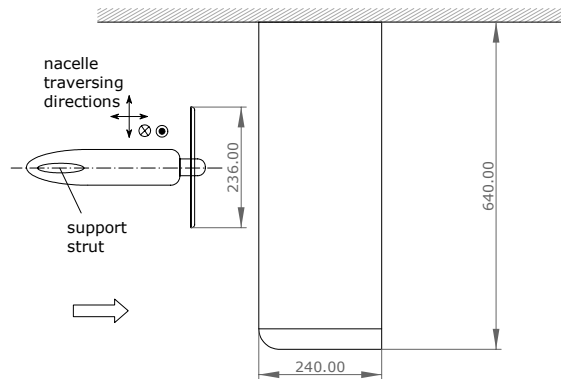


Fig. 3 Dimensions and layout of the APROPOS model.

propeller position is $y_p/b/2 = 0.469$. A sketch is presented in Fig. 4.

The second windtunnel model referenced as APROPOS (Fig. 3) is identical with PROWIM except for the fact that the nacelle is detached from the wing. The nacelle is supported by a strut which can be traversed with the 3-component traversing system mentioned earlier. In the APROPOS layout the separate effect of the propeller position relative to the wing was investigated.

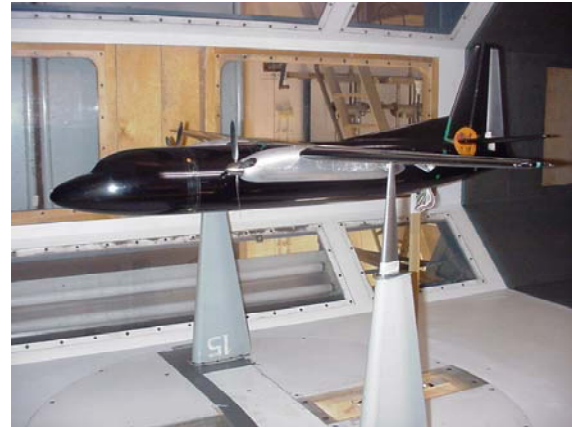


Fig. 5 Fokker F27 scale model in the Delft University low speed windtunnel.

4.2.2 F27 aircraft model

This model is a 1:20 scale model of the prototype of the Fokker F27 aircraft (Fig. 5). The model consists of several parts that can be detached for detail tests. The span of the high aspect ratio wing ($A = 12$) is 1.45 m.

5 Results

The results of some calculations and experiments will be discussed on the basis of the geometrical aspects of the configuration as well as the wing and propeller modeling techniques employed in the analysis. Where possible, the numerical results will be compared directly with the experimental results.

5.1 Propeller rotation effect

As suggested by Veldhuis [9], Miranda [1] and Kroo [11] the propeller inboard up (IU) rotation is beneficial since the wing the magnitude of the lift vector at the nacelle inboard side that is tilted forward is higher than the backward tilted vector at the nacelle outboard side. This effect was confirmed by our calculations and experiments as indicated in Fig. 6 to Fig. 10.

In Fig. 6a, a small lift increased can be noticed for the PROWIM model due to the propeller inboard up running propeller slipstream running against the wing tip vortex. More pronounced however is the effect on the (effective) drag coefficient, C'_D presented in Fig. 6b.

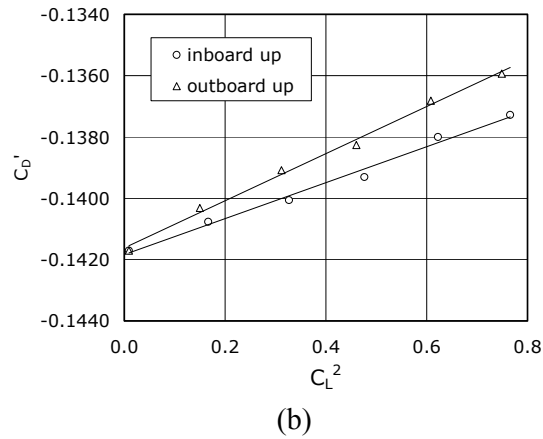
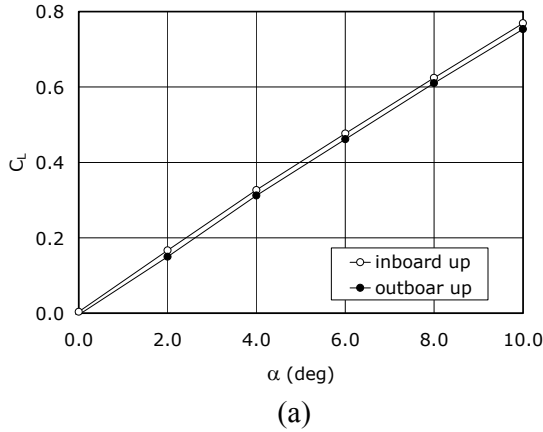


Fig. 6 Effect of propeller rotation direction on the lift coefficient (a) and the drag coefficient (b) of PROWIM ; $J = 0.85$.

The positive power effect on the lift is found also for the F27 aircraft model (Fig. 7)

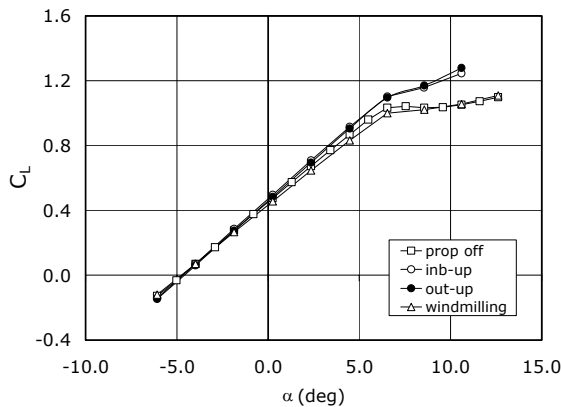


Fig. 7 Effect of propeller rotation direction and wind milling on the lift curve of the F27 model;

$Re_c = 0.41 \cdot 10^6$; $T_c = 0.127$; $\beta_{0.75R} = 25^\circ$.

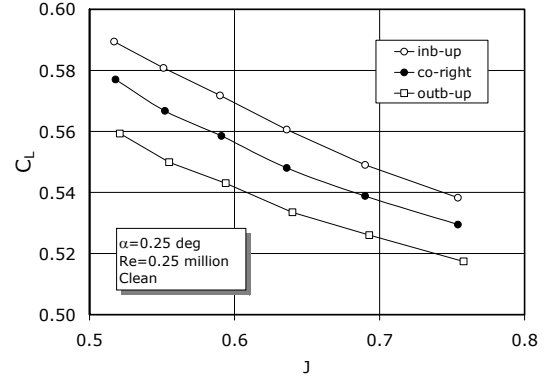


Fig. 8 Effect of the propeller rotation direction and the advance ratio on the lift coefficient of the F27 model ; $\alpha = 0.25^\circ$.

Even if the propeller's distance from the wing tips is large for the F27 model its influence on the effective aspect ratio of the wing apparently is still noticeable. The difference of both the prop-on cases with prop-off case again arises from the contribution of the increased dynamic pressure in the slipstream area and the propeller normal force. As expected the wind milling case (co-right) produces the lowest lift curve slope due to the strong dynamic pressure loss in the slipstream.

The effect of the thrust coefficient for a constant angle of attack of $\alpha = 0.25^\circ$ is presented in Fig. 8. Although the effects are relatively small the outboard up (OU) rotating propeller clearly shows the lowest increase in the lift coefficient. The effect of the rotation direction on the lift-drag polar is presented in Fig. 9. It should be noted that the "drag coefficient", along the x-axis, incorporates the thrust. Therefore negative C_D -values are found. The effect of the propeller rotation direction on the drag coefficient confirms the (small) beneficial effects of the inboard up rotating propeller. At a typical cruise lift coefficient of $C_L = 0.4$ the difference between the outboard up and the inboard up rotating propeller is 4 drag counts in favor of the latter. The difference between the two propeller rotation cases depends on the lift coefficient. One may expect that with increasing lift acting on the wing, the relative effects of the opposite swirl distribution introduce larger changes in the drag. Fig. 10 shows that the positive influence

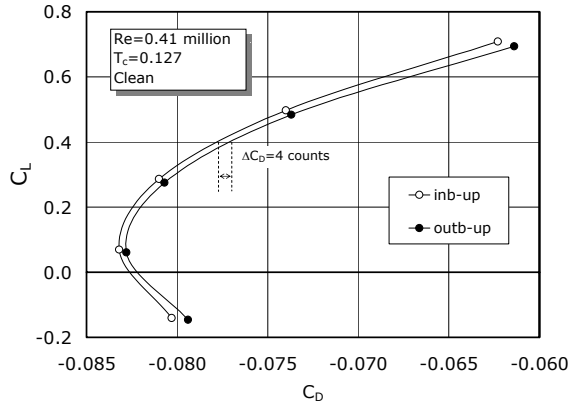


Fig. 9 Lift-Drage polar for the F27 at $T_c = 0.127$ in the clean configuration.

of the inboard up rotation indeed increases for the higher C_L values.

The effect of the rotation direction was investigated also with the enhanced VLM-code. The calculations were based on a Fokker 50 like configuration. The most important results are summarized in Table 1. The data are analyzed based on the propulsive efficiency that is defined as:

$$\eta_p = \frac{-C_{D_{tot}}}{P_c} \quad (2)$$

Here $C_{D_{tot}}$ is the total drag coefficient corrected for the thrust of the propeller and P_c is the power coefficient.

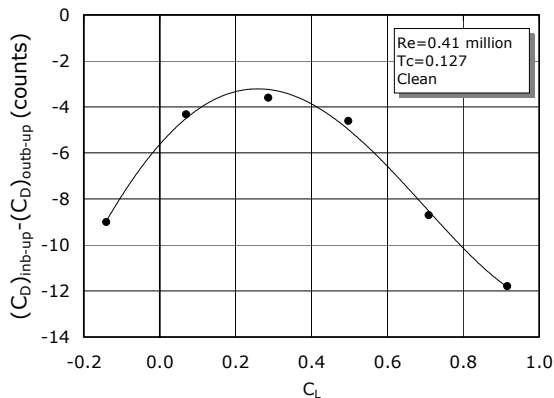


Fig. 10 Difference in drag coefficient for the inboard up and the outboard up rotation case ; F27 in clean configuration.

Table 1 Influence of propeller rotation direction on the lift coefficient and the effective propulsive efficiency; Fokker F50 configuration.

| High speed case | | |
|--------------------|--------|-------------------|
| Rotation direction | C_L | $(\eta_p)_{corr}$ |
| inboard up | 0.4986 | 0.38550 |
| co-right | 0.4974 | 0.38466 |
| outboard up | 0.4962 | 0.38388 |
| Low speed case | | |
| Rotation direction | C_L | $(\eta_p)_{corr}$ |
| inboard up | 1.2468 | 0.41577 |
| co-right | 1.2439 | 0.41518 |
| outboard up | 1.2408 | 0.41458 |

The IU case indeed produces the highest propulsive efficiency for both a typical low speed and a high speed flight condition but the magnitude of the effects is rather small. The propulsive efficiency for the IU case is only 0.23% higher than for the (conventional) CR-case for the high speed (cruise) condition. For the low speed case this even reduces to 0.14% in favor of the IU-configuration. These values are considerably lower than expected from earlier experiments and calculations on optimized wing geometries [12]. Nevertheless, for wing configurations with a much lower aspect ratio or with a wider propeller (i.e. higher value of D/b) the differences between the IU and the OU case are likely to increase.

5.2 Streamwise propeller position

By changing the propeller streamwise position referenced to the wing location the aerodynamic coupling between the two elements change. The swirl velocity maintains its value obtained directly behind the propeller plane while the axial velocity at the wing increases considerably with increasing distance, x_p , between the propeller and the wing.

Ref. [13] presents results of windtunnel test that were on a full 3D-aircraft model with the propeller located at $0.25c$ and $0.40c$ ahead of the wing leading edge. It was found that the installations with the propeller close to the wing were more efficient than the configuration. To

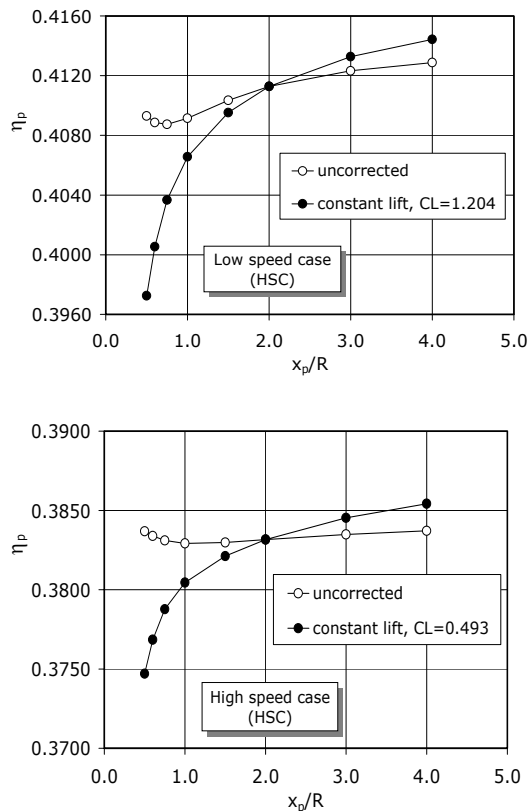


Fig. 11 Propulsive efficiency versus the propeller streamwise position of Model-1 for a typical low speed and high speed case taking the full interaction of the propeller and the wing into account.

verify these findings the effect of different streamwise positions was analyzed for the Fokker 50 like configuration, further denoted as Model-1, using the VLM-method.

Both a typical high speed case ($J = 1.63$, $T_c = 0.046$) and a low speed case ($J = 1.00$, $T_c = 0.251$) were used for this analysis.

Evidently the streamwise position of the propeller affects to some extent the propulsive efficiency, η_p , as indicated by Fig. 11. The open symbols indicate the trend in case the propeller position is changed without taking notice of changes in the wing lift, while the line with the closed symbols show the data points that were corrected to a constant lift coefficient. When the propeller is brought closer to the leading edge of the wing, the upflow in the propeller plane changes. This in turn leads to a distortion of the velocity distributions in the slipstream. The

result is a change in the wing lift and in the drag distribution that directly influences the efficiency of the propeller-wing configuration. It should be remembered here that in these calculations the full interaction between the propeller and the wing was modeled (FIM).

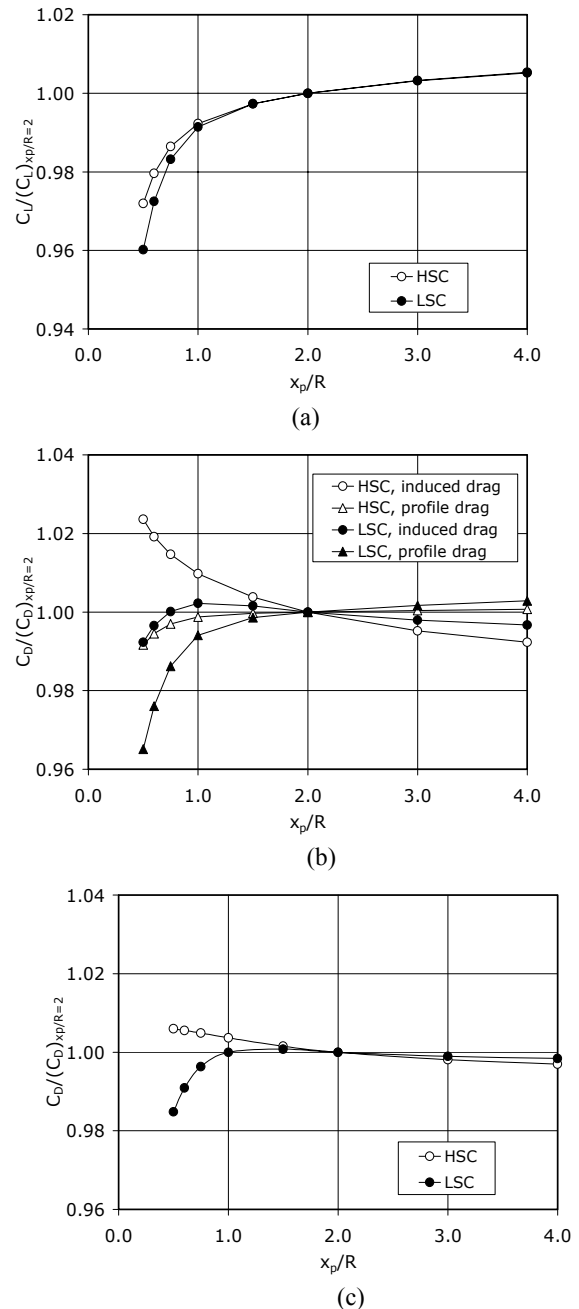


Fig. 12 Effect of propeller streamwise position on the wing of model 1 for the low speed case (LSC) and the high speed case (HSC); (a) the lift coefficient; (b), the drag coefficient components; (c) total drag coefficient

The source for the slightly higher propulsive efficiency with increasing distance to the wing LE can be found in the higher lift coefficient due to the augmented dynamic pressure at greater distances from the propeller disk. This effect is depicted in Fig. 12a where the ratio between the lift coefficient for a given propeller position and the one found at $x_p/R=2.0$ is given. Although the slipstream velocity distributions are quite different for the low speed case (LSC) and the high speed case (HSC) the ratio $C_L/(C_L)_{x_p/R=2.0}$ changes almost identically with x_p . The change in the drag coefficient with x_p (Fig. 12b) is split into the two main contributors: profile drag and induced drag.

The profile drag component exhibits the same behavior for both thrust cases in that increasing x_p results in higher C_{D_p} values due to dynamic pressure effects (increased "scrubbing drag"). However the induced drag runs in a different way when the propeller approaches the wing. In the low speed case the thrust force is relatively high and the propeller induced velocity components compared to the undisturbed velocity are higher than in the high speed case. This apparently leads to stronger propeller induced angle of attack effects for the propeller that is in close proximity of the wing. From $x_p/R=1.0$ on both C_{D_i} curves show a negative gradient which could be anticipated since due to the higher local lift coefficient, in the slipstream washed area of the wing, stronger swirl recovery due to the presence of the wing occurs. When the total drag coefficient is calculated versus x_p a small change is found, however.

The range over which the propeller was translated was chosen rather wide to be able to identify the streamwise effect as complete as possible. For practical reasons however the choice for the propeller streamwise position is constrained by the space needed for the engine in relation to the wing structural layout. Therefore the variation of x_p is to be seen only as an "aerodynamic test case" without concerning the problems related to the nacelle-

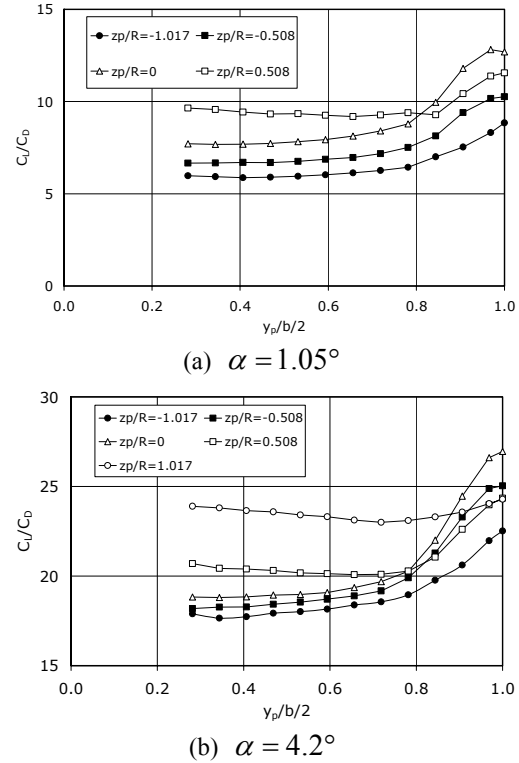


Fig. 13 Effect of the propeller spanwise location, y_p , on the lift/drag ratio of the APROPOS wing for several vertical propeller locations, z_p ; $J = 0.92$; $T_c = 0.127$; $\alpha_p = 0^\circ$.

wing structure. Still, in a practical range of $x_p/R=1.5-2.0$ a small effect on the propulsive efficiency is found. One may conclude that from the fuel consumption point of view a propeller position not too close to the wing leading edge is beneficial.

5.3 Spanwise propeller position

The spanwise gradient lift distribution at the position where the slipstream washes the wing plays an important role with respect to the possible performance benefits introduced by the propeller. This was already shown by in earlier investigations [1,9,11]. The influence of the spanwise propeller position was investigated using the APROPOS test setup. In Fig. 13 and Fig. 14 the effects of the spanwise position is presented for a rather low thrust condition.

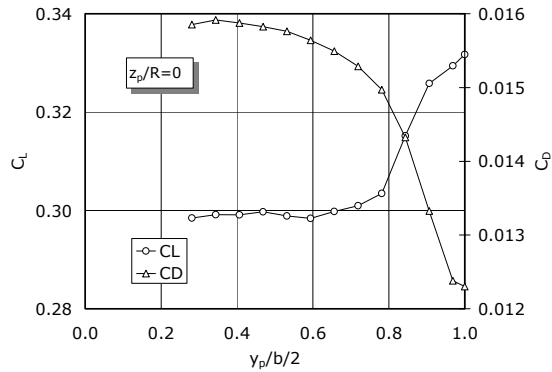


Fig. 14 Effect of the propeller spanwise location, y_p , on the lift and the drag coefficient of the APROPOS wing; $J = 0.92$; $T_c = 0.127$; $\alpha_p = 0^\circ$; $\alpha = 4.2^\circ$.

The different curves in these figures correspond to different vertical positions of the propeller, which will be discussed in a subsequent section. As expected the performance of the wing improves when the propeller is moved in the direction of the wing tip indicated by the increasing wing lift / drag ratio.

The reason for this change in the lift / drag ratio can be found in a increase in the lift coefficient combined with a concurrent reduction of the drag coefficient towards the tip, as indicated by the curves in Fig. 14.

Apparently the vorticity field (swirl) induced by the inboard up rotating propeller attenuates the wing tip vortex influence. As a result, the effective aspect ratio of the wing is increased which leads to the lift increase and drag decrease. Tests at several angles an attack and vertical propeller positions have shown that the effect at the wing tip is maximum when the slipstream centerline is exactly in line with the wing tip vortex. Although the spanwise propeller position strongly affects the performance for positions close to the wing tip, it should be remarked that small changes in y_p for realistic positions ($0.25 < y_p/b/2 < 0.30$) shows negligible changes.

The effect of the spanwise propeller position was analyzed with the VLM-code based on Model-1. To keep the configuration more

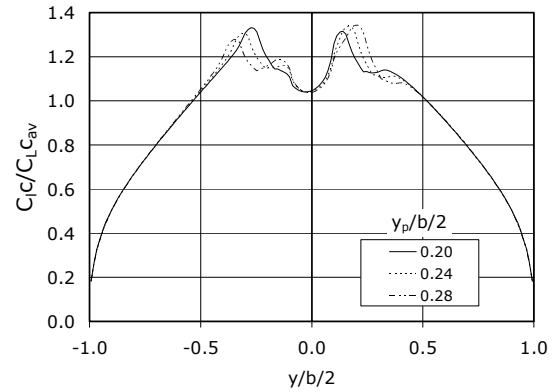


Fig. 15 Spanwise loading distribution for three lateral propeller positions; Model-1; high speed case.

realistic than considered in the experimental campaign for APROPOS, the spanwise propeller position was changed over a small range of $y/(b/2) = 0.20 - 0.28$ only. The spanwise loading distributions are presented in Fig. 15 while the characteristic coefficients are given in Table 2.

The small shift in the propeller position is clearly visible in the spanwise loading given as $C_l/C_{L_{av}}$ versus $y_p/b/2$. Although the most outboard position produces a somewhat higher propulsive efficiency, as expected, the differences between the 3 positions are too small to be of significance for the design process. This result can be attributed to the fact that the lift distribution is rather flat for the given propeller position.

Table 2 Influence of spanwise propeller position on the lift coefficient and the effective propulsive efficiency of Model-1.

| High speed case | | |
|-----------------|--------|-------------------|
| $y_p/(b/2)$ | C_L | $(\eta_p)_{corr}$ |
| 0.20 | 0.5459 | 0.35209 |
| 0.24 | 0.5464 | 0.35210 |
| 0.28 | 0.5466 | 0.35226 |
| Low speed case | | |
| $y_p/(b/2)$ | C_L | $(\eta_p)_{corr}$ |
| 0.20 | 1.2965 | 0.39967 |
| 0.24 | 1.2955 | 0.39966 |
| 0.28 | 1.2929 | 0.39984 |

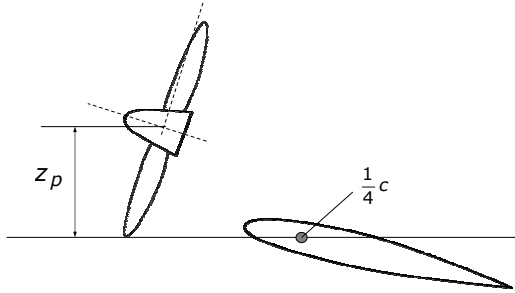


Fig. 16 Definition of the vertical propeller coordinate, z_p .

5.4 Vertical propeller position

Since twin-engined turboprop aircraft show quite different vertical propeller positions with reference to the wing, the z_p coordinate (Fig. 16) was changed in the APROPOS tests to investigate the performance effects.

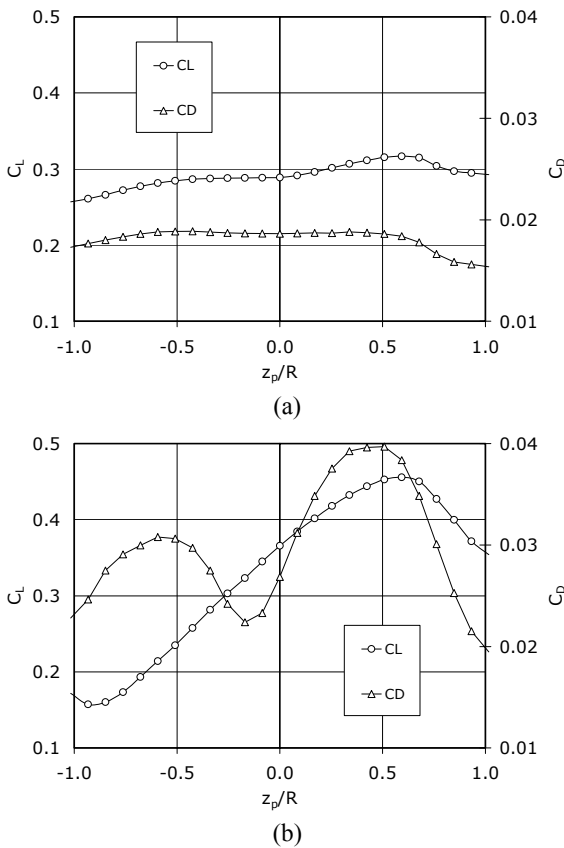


Fig. 17 Effect of propeller vertical position on the lift and drag coefficient of the APROPOS wing at $\alpha = 4^\circ$; (a) low thrust ($T_c = 0.137$); (b) high thrust ($T_c = 0.985$)

The tests showed that the vertical propeller position has a remarkable effect on the performance of the wing. For realistic spanwise locations of the propeller a high position is beneficial with respect to the wing lift/drag ratio, mainly due to a lift enhancement induced by the combination of dynamic pressure increase at the wing's upper surface and contraction of the slipstream which leads to increased flow angles of attack.

In Fig. 17 the effect of the vertical propeller position on the APROPOS lift and drag coefficient is depicted.

Whereas only moderate changes in C_L and C_D occur for the lower thrust coefficient a more pronounced effect of the propeller slipstream can be noticed for the higher thrust case.

The local drag minimum for the mid position of the propeller is likely to be caused by the fact that for z_p values close to zero a smaller part of the immersed part of the wing is washed by the slipstream annulus that contains increased dynamic pressure ("doughnut" effect). This principle is illustrated in Fig. 18.

The increase in the lift coefficient that is found when the propeller is moved from negative to positive Z_p values, is attributed to the effect of the contraction of the slipstream. For high z_p/R values this results in a local wing angle of

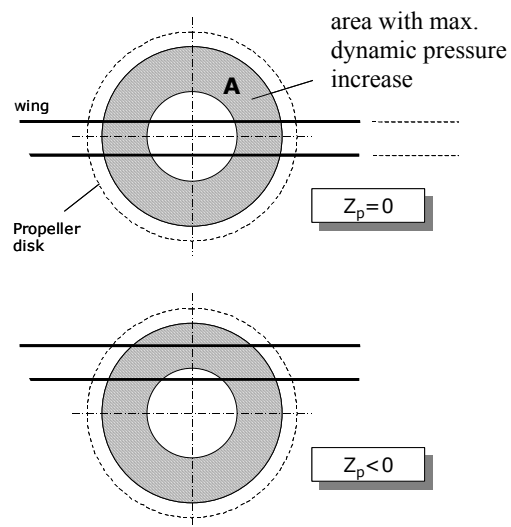


Fig. 18 Increase in average dynamic pressure increase over the wing due to off-centre position of the propeller ($z_p \neq 0$).

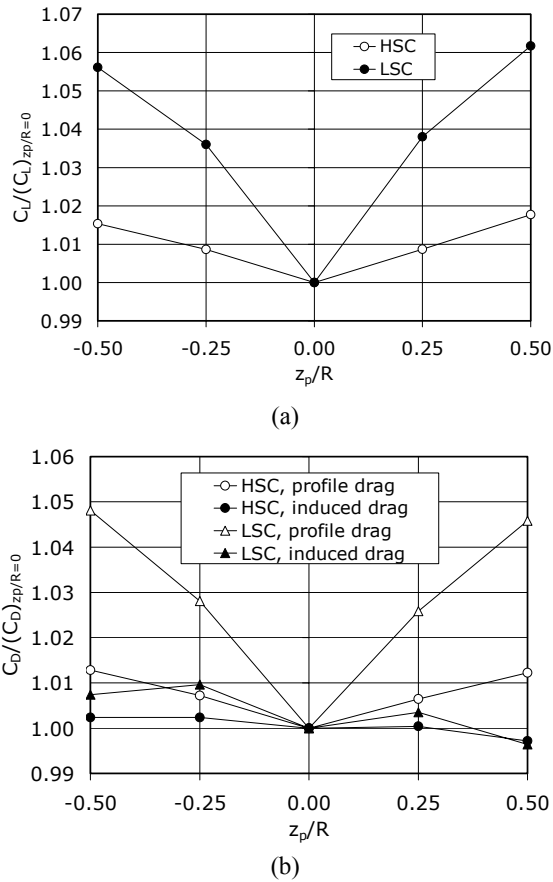


Fig. 19 Calculated effect of vertical propeller position on the lift coefficient (a) and the drag coefficient (b) of Model-1 calculated for the high speed and the low speed case.

attack increase and a lift increment; for the lower z_p/R values an opposite effect occurs.

Considering these results one can state that the wing may benefit from the presence of the propeller since C_L/C_D rises for the higher propeller positions. The trends that were found experimentally seem to confirm the (limited) observations by other researchers that the projection of the propeller plane onto the wing strongly influences the local wing lift.

To study the effects of the vertical position further VLM-simulations were conducted on Model-1 for a range of $z_p/R = -0.5 \rightarrow 0.5$. This range is somewhat beyond that found for typical twin powered propeller aircraft. It is obvious that values $|z_p/R| > 0.25$ lead to very low/high

nacelles. This in turn might then lead to excessive high nacelle-wing interference drag. The effects of the vertical propeller position were examined by selecting 5 positions spaced $0.25R$ apart; assuming that no significant changes would occur for intermediate positions.

Fig. 19 gives an impression of the effect of z_p on the lift and the drag coefficient. The results are expressed in the form of a ratio between the values found at the specific location and $z_p/R = 0$. The first thing that can be noticed is the minimum in the lift coefficient found at $z_p/R = 0$. Apparently the overall dynamic pressure increase over the wing part immersed in the slipstream increases somewhat when the propeller is put at an off-zero position. The drag coefficient is mostly affected by a change in the profile drag component showing variations up to 5% while the induced drag alters not more than 1% for the given range of propeller positions.

Comparing the data of Fig. 19 with the earlier found data for PROWIM the VLM-code overestimates the lift coefficient for the low propeller positions. A possible cause for this is twofold. Firstly the inflow into the slipstream, which determines the local wing angle of attack, may be not modeled correctly. A second cause for this discrepancy is very likely the result of the code's inability to take the slipstream deformation into account. From the experimental investigations on PROWIM a considerable deformation was found. Neglecting this phenomenon introduces different slipstream velocities to the wing apparently causing some asymmetry in the lift and drag distributions with reference to the $z_p/R = 0$ position.

Since the effective propulsive efficiency is directly correlated with the total lift and drag values, a more acceptable value of η_p can be obtained by applying a correction such that the lift coefficient resembles that of Fig. 17 i.e. lower values for negative z_p . The original and the (lift) corrected values of η_p are presented in Fig. 20. It is remarkable to notice that, in

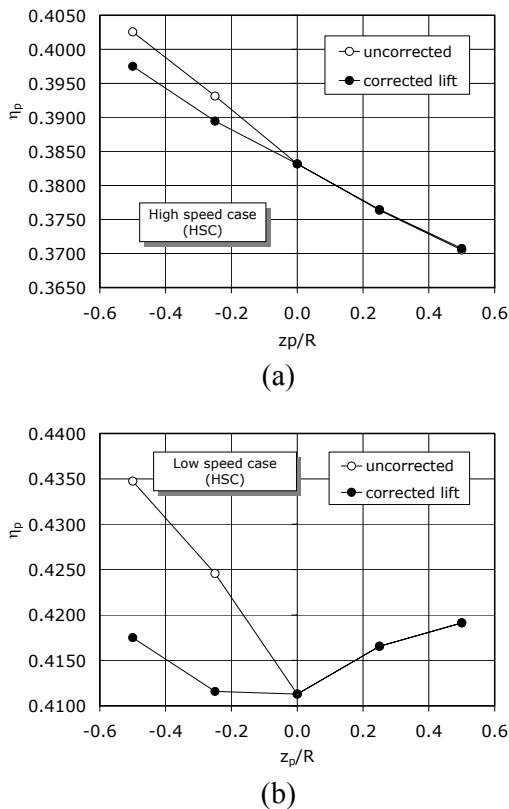


Fig. 20 Uncorrected and –lift corrected values of the effective propulsive efficiency versus the vertical propeller position; high (a) and low (b) speed case for Model-1; VLM.

contrast with the lift and drag distributions for both the uncorrected and the lift-corrected case no symmetry with respect to $z_p / R = 0$ is found.

Especially the high speed case, which is representative for the cruise condition of the aircraft, shows a considerable higher propulsive efficiency for the low propeller positions. Again it should be made clear that the statements presented with respect to the vertical propeller position are considered only from the propeller-wing aerodynamics point view. No conclusive remarks can be made regarding the best position when both structural and stability and control aspects are taken into account as well. Separate investigations, incorporating interference between aerodynamic and structural loads are needed for this enhanced design analysis, which fall outside the scope of this paper.

5.5 Propeller angle of attack effect

Significant flow non-uniformity might be introduced in the propeller plane due to wing induced upwash as well the presence of the nacelle (positioned at a non-zero angle of attack). The fact that this has a negative effect on the propeller is another reason to explore the possible advantageous effects of a Propeller-Tilt-Down configuration, further denoted as PTD.

Normally the angle of incidence given to a propeller is limited to say 2° which effectively reduces the cyclic loading due to the wing upwash generated skewed flow field. To experimentally verify the possible performance effect of PTD configurations much bigger angles were analyzed. Although all the tests were performed for different y_p and z_p values combined with several propeller incidence angles, α_p , only the experimental results for

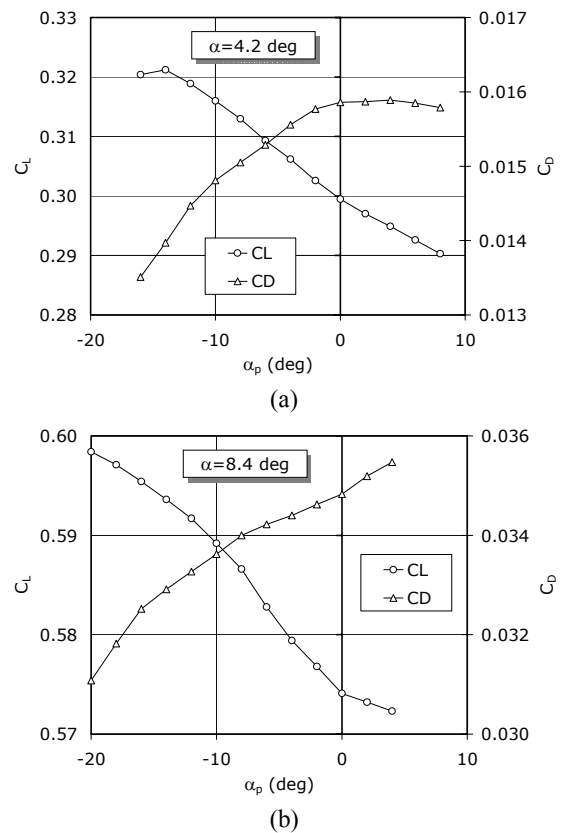


Fig. 21 Effect of propeller angle of attack on the wing lift and drag coefficient of APROPOS; (a) $\alpha = 4.2^\circ$; (b) $\alpha = 8.4^\circ$; $J = 0.92$

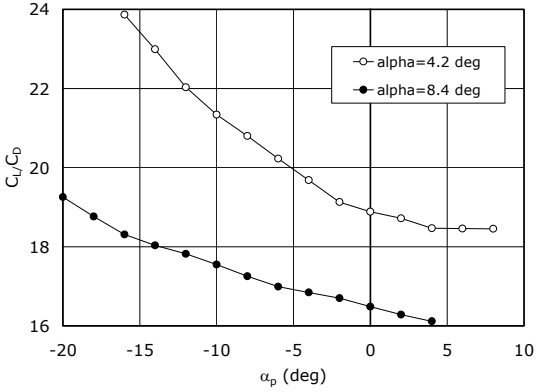


Fig. 22 APROPOS wing lift/drag ratio versus the propeller angle of attack relative to the wing chord reference line; $J = 0.92$.

$y_p / b / 2 = 0.469$ and $z_p / R = 0$ will be presented here.

In Fig. 21 the lift and the drag coefficient of the APROPOS model are given versus the propeller angle of attack, α_p .

The tilting-down of the propeller evidently leads to improved performance of the wing through an increase in the lift and a significant decrease in the drag. This causes in a notable rise of the lift / drag ratio, as indicated in Fig. 22. Note that the underlying cause is on principal different from the effect of vertical displacement of the propeller since now the velocity distribution in the slipstream has undergone a major change [9].

Furthermore the (small) negative normal force acting in the propeller plane and the (small) reduction in effective thrust hardly reduces the positive effects of the PTD.

The remarkable strong effects of α_p were also analyzed with the VLM-code using the more realistic Model-1. Fig. 23 shows the build-up of the lift coefficient. For decreasing propeller angle of attack the wing lift increases slightly due to the upwash encountered by the wing immersed in the slipstream.

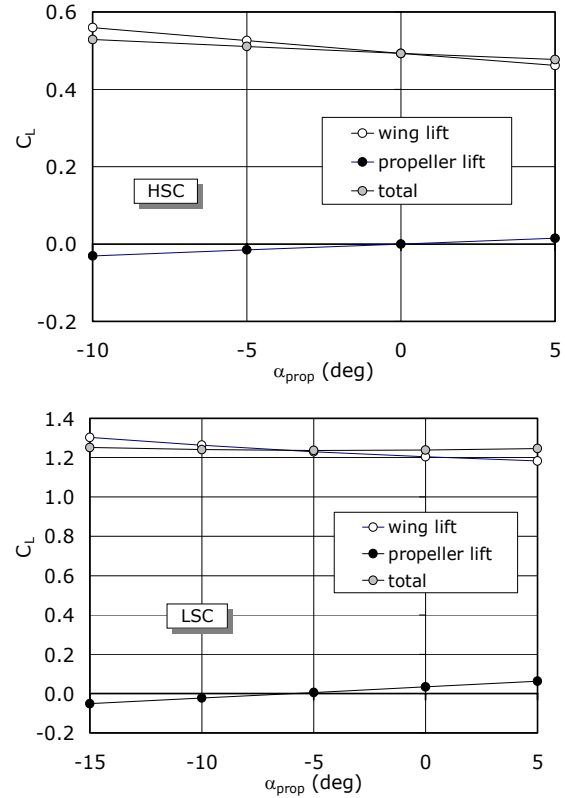


Fig. 23 Components of the lift coefficient for Model-1 versus the propeller angle of attack; (a) high speed case; (b) low speed case.

However, the direct lift force that acts on the propeller (denoted 'propeller lift') lowers the total lift as a result of tilting down the thrust vector and the negative propeller normal force that is associated with negative α_p . The trend for both the high speed case and the low speed case is similar though the changes due to α_p are somewhat stronger for the latter.

To compare the α_p -effects on the lift and the drag, ratios were defined taking the values at $\alpha_p = 0^\circ$ as a reference. Fig. 24 shows the results for C_L and C_D , where the latter again is split in the two separate contributors: profile drag and induced drag.

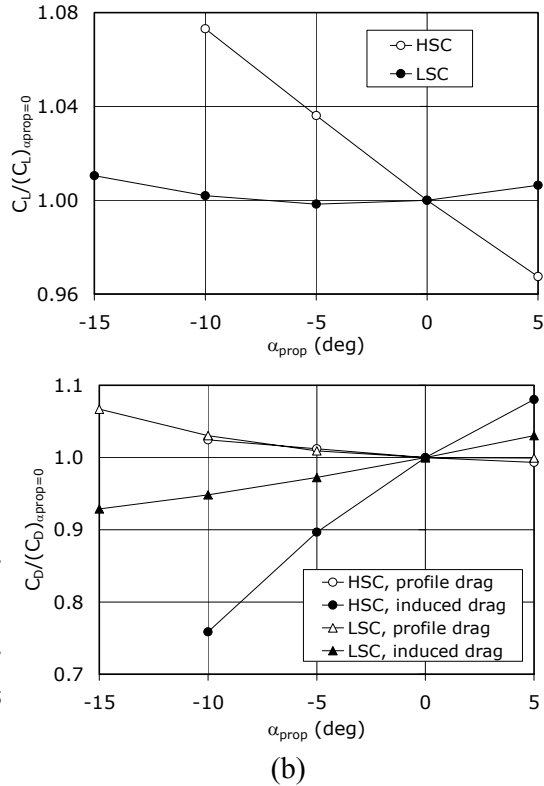


Fig. 24 Effect of propeller angle of attack on the lift (a) and drag (b) ratios for Model-1. The values at $\alpha_p = 0^\circ$ were taken as a reference.

Small increments in the lift coefficients are found in the low speed case with decreasing α_p while more significant effects are predicted for the high speed case. In the latter case the most prominent contribution is due to the change in the wing lift. By lowering the advance ratio, as is done in the low speed case, the relative contribution of the propeller normal force increases leading to a smaller change of C_L with decreasing α_p .

The picture for the drag coefficient becomes more complex since the total “drag” force is constituted of 3 components: profile drag, induced drag and propeller “drag” (in fact thrust).

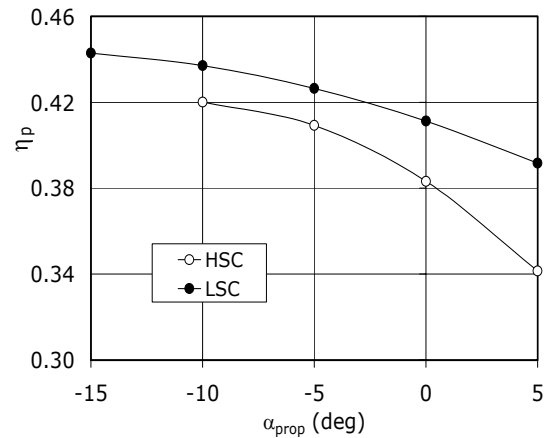


Fig. 25 Propulsive efficiency of Model-1 versus the propeller angle of attack for the high speed and the low speed case.

In Fig. 24b the drag ratio $C_D / (C_D)_{\alpha_p=0}$ is shown for both flight cases. Once more the effect of lowering the propeller angle of attack is more pronounced for the high speed case. That is: the relative change in the drag coefficient is higher which is of course to be partially contributed to the lower absolute values of the drag coefficient in this case. The change in the profile drag coefficient is negligible, which could be expected from the fact that the average dynamic pressure in the slipstream is almost not affected by changes in the propeller angle of attack. The induced drag, on the other hand, diminishes expressively as a consequence of the increased upflow in front of the wing. As discussed earlier, the increased upwash tilts the force vector acting on the wing forward which moderates the induced drag.

The combined effects on the changed lift and drag contributions leads to favorable propulsive efficiencies for low values of α_p , as indicated by Fig. 25. In the high speed (cruise) case η_p rises approximately 9.5% by changing α_p from 0° to -10° . This performance improvement is interesting enough to be considered further in design studies of tractor propeller wing configurations.

5.6 Numerical modeling complexity

The problem of propeller wing interference needs prediction codes which incorporate all important aspects as discussed above. To be able to determine to what level of complexity the prediction codes should be developed to acquire acceptable calculation results, the two numerical methods will be discussed briefly.

5.6.1 VLM method

The significance of completing the full interaction scheme, e.g. take into account the propeller effects on the wing and vice versa, was assessed by comparing the final results of step 1 (no wing effect on the propeller) and step 2 (full interaction) in the VLM approach.

The primary indication whether the full interaction is needed is found from a comparison between the lift distributions found for both situations. In Fig. 26 this is expressed in the form of a difference between the local lift coefficient found for step 1 and step 2, ΔC_l . Again the calculations were performed for both the high speed and the low speed case.

Apparently a significant difference exists between the results of the calculation without interaction and the full interaction case. The differences are especially found in the vicinity of the propeller where the effect of the slipstream is the most prominent. The fact that larger values of ΔC_l are found for the low speed case is trivial since for this condition a higher lift is produced by the wing which causes a stronger deterioration of the inflow field of the propeller.

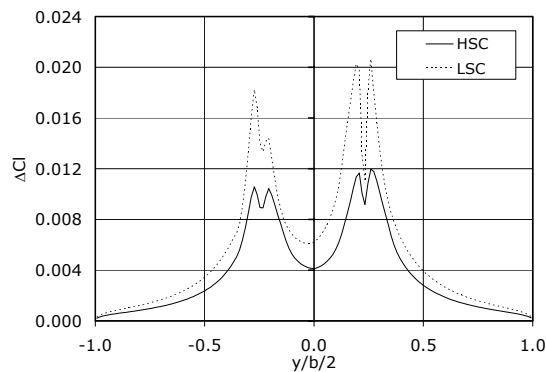


Fig. 26 Difference between the local lift coefficient distribution of step 1 (no interaction) and step 2 (full interaction) calculation on Model-1 for the high (HSC) and the low speed case (LSC).

From the data found it may be concluded that all propeller-wing calculations should be performed in the full interaction mode (FIM). The propulsive efficiency changes 0.3%–1.0% for the high speed while a 0.7%–2.5% change is found for the low speed case. The suggestion, offered by some authors, that the wing effect on the propeller, in case of the tractor propeller located well ahead of the wing, can be neglected should therefore be questioned.

In Fig. 27 the lift coefficients of two experiments are compared with the VLM-data.

As can be seen an excellent agreement between the three methods is found. Apparently the VLM-method predicts the propeller effects on the overall lift coefficient of the configurations

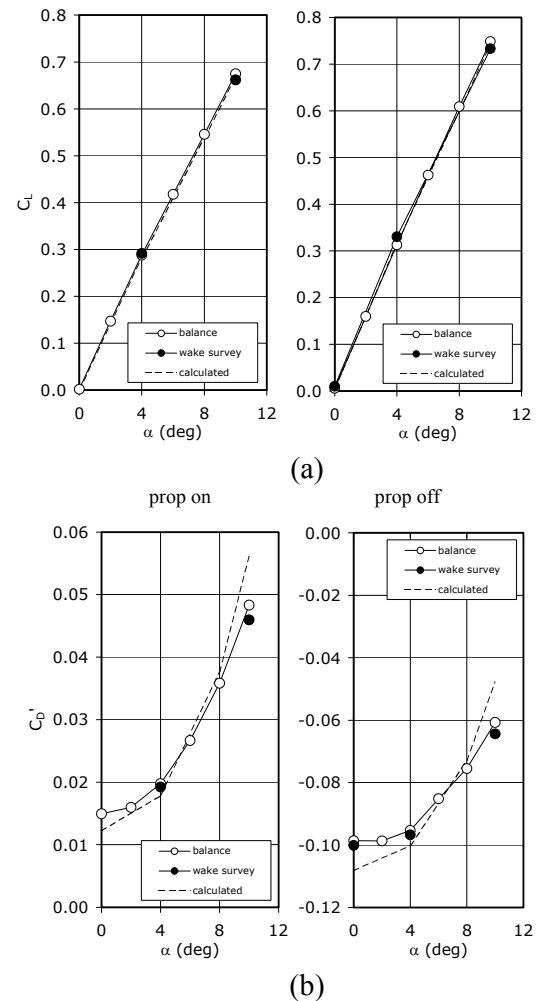


Fig. 27 Comparison of experimental and predicted lift (a) and drag (b) coefficient (VLM) of PROWIM.

accurately.

In general an accurate value of the drag coefficient is very difficult to capture due to difficulties in the estimation of the profile drag. Nevertheless the VLM-code gives a reasonable prediction of the total drag coefficient, as can be seen in Fig. 27. The differences compared to the experimental values are likely to be caused by inaccuracies in the profile drag data read by the VLM-code. The fact that a reasonable agreement is found supports the conclusion that the typical propeller effect; a drag rise in the propeller washed area due to dynamic pressure increase, is effectively envisaged by the code.

The capabilities of the VLM-code can be further be acknowledged by comparing the calculated spanwise loading with experiments and other

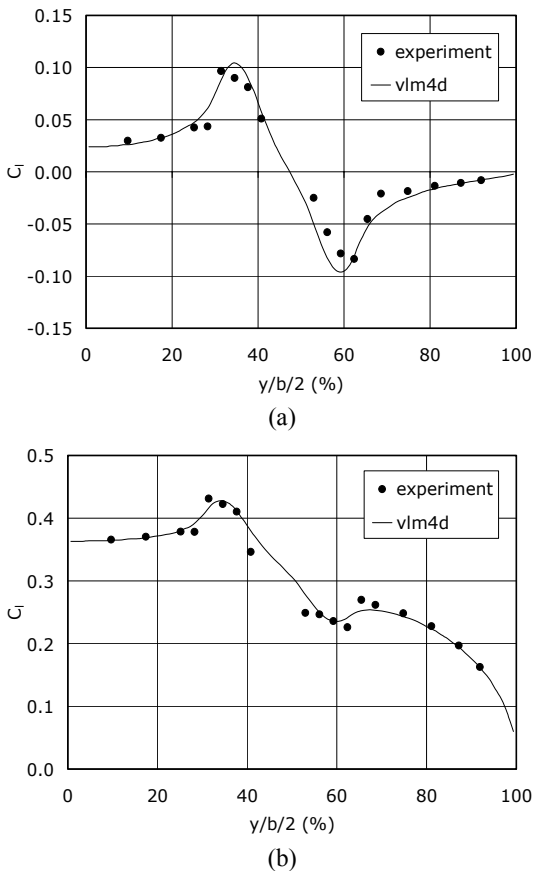


Fig. 28 Comparison of the experimental and the calculated lift distribution from the PROWIM experiment; propeller rotating inboard up; $J = 0.85$; $T_c = 0.168$; (a) $\alpha = 0^\circ$; (b) $\alpha = 4^\circ$.

codes.

In Fig. 28 some results for the PROWIM model are compared.

The agreement is very acceptable for both angles of attack and a clear deformation of the elliptic-like shape as a result of the slipstream swirl velocity component is found. The sharp changes in the experimental lift distribution are softened to some extent by the code, possibly as a result of an inaccurate calculation of the true slipstream velocities (BEM analysis).

It should be remarked that the VLM-calculations were performed with an swirl recovery factor of about $SRF = 0.5$. As is found with many codes that do not incorporate an SRF , ignoring the effect of swirl recovery leads to overestimated propeller slipstream effects on the wing.

Additional verification of the predictive capabilities of the VLM-code were performed by comparing results obtained from flight tests [14]. During these test the lift distribution over the wing was obtained by performing pressure measurements in chordwise direction using pressure belts. Two typical flight conditions were considered to wit: a low thrust case (LTC) with $\alpha = -0.2$, $T_c' = 0.63$, $J = 1.0$ and a high thrust case (HTC) where $\alpha = -0.2$, $T_c' = 0.63$. Fig. 29 shows the comparison between the experimental values, the VLM-approach and the results obtained with an dedicated Euler code [15]. The VLM code shows a remarkable good agreement with the other data, including the local effect of the nacelles and the fuselage. Unmistakably the application of the SRF prevents unrealistic swirl velocity effects in the wing part washed by the propeller slipstream.

The main disadvantage of the VLM-method is unmistakably the limited level of detail that is obtained. Since only integral characteristics are obtained the possibilities to verify the flow phenomena in detail with available data is impossible.

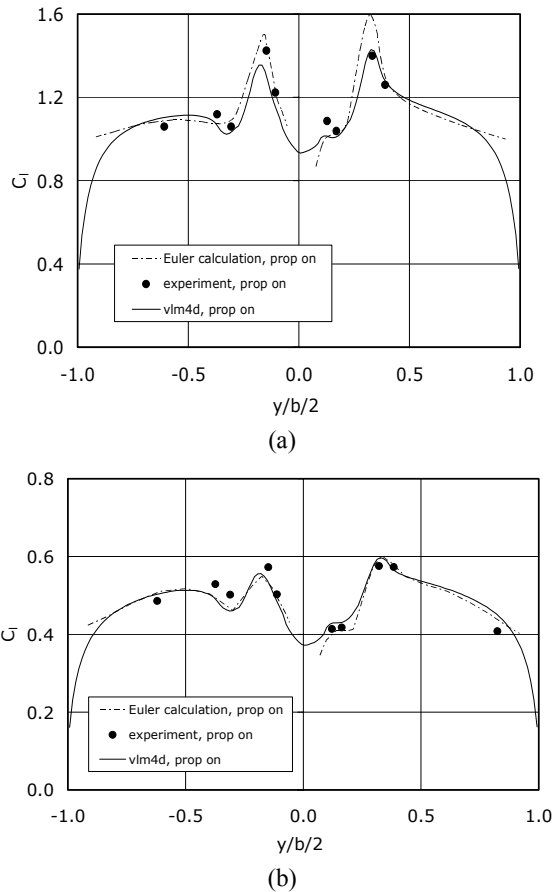


Fig. 29 Spanwise lift distributions found with an advanced Euler code [15] and the VLM-method compared with experimental results [14]; Fokker-50 in the low thrust case; (a) HTC; (b) LTC.

5.6.2 NS-approach

The advantage of higher order calculations codes is to be found in the possibility to determine the chordwise pressure distribution in more detail. However, some calculations on the PROWIM model that were performed with a panel code [16] revealed the problem with correct definition of the relation between the propeller loading and the slipstream induced flow properties at the location of the washed wing panels.

The main cause for the discrepancy between the experimental and the numerical results of panel codes is the omission of the viscous effect (no decambering effect) and the lack of a swirl recovery factor (that must be set by the user). The panel code's inability to predict the secondary flow phenomena, like flow boundary

layer thickening and small areas of flow separation that were found in the experiment, led to the conclusion that the intermediate step in calculation complexity (panel codes) is not interesting for a quick or accurate prediction of propeller-wing interaction effects. Hence the Navier-Stokes calculations were set up for the PROWIM model.

As expected, a much better agreement with experimental data were found.

Some results are presented in Fig. 30 to Fig. 32.

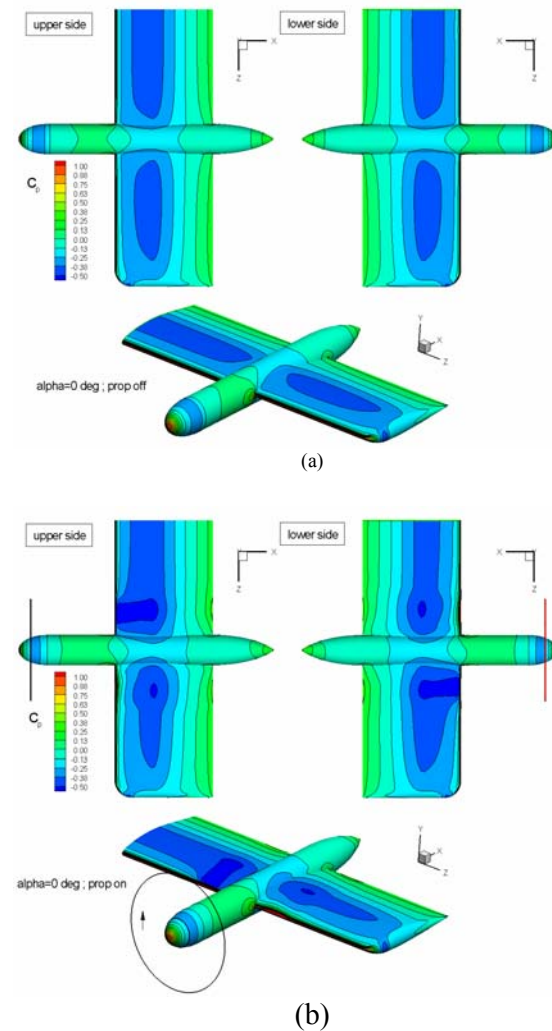


Fig. 30 Calculated surface pressure distribution of PROWIM; $\alpha = 0^\circ$; (a) prop off; (b) prop on.

The pressure distributions in Fig. 30 clearly show the effect of the propeller slipstream that washes the wing. Especially the impact of the swirl velocity component is very pronounced. The capability of the NS-code to incorporate the

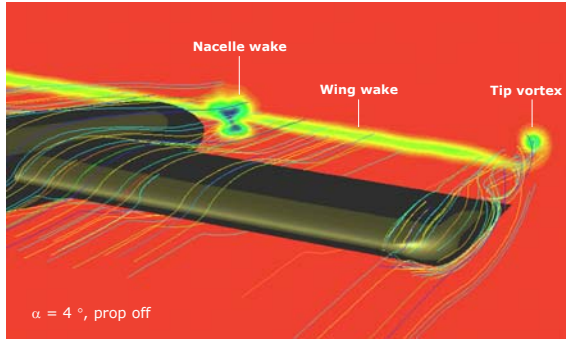


Fig. 31 Combined flow path lines and contours of total pressure loss behind showing the wake and the tip vortex structure; $\alpha = 4^\circ$; prop off.

deformation of the wing wake and the slipstream, as sketched in Fig. 31 and Fig. 32 respectively, is essential for a detailed analysis of the propeller-wing interactive flow.

The strongest point of the NS-code in the analysis of the propeller-wing interaction problem is its intrinsic modeling of the swirl recovery effects. Furthermore, no user intervention is needed to prescribe the slipstream position within the computational domain.

Integration of the surface pressure and friction forces leads to a very acceptable agreement with experimental values found earlier (Table 3).

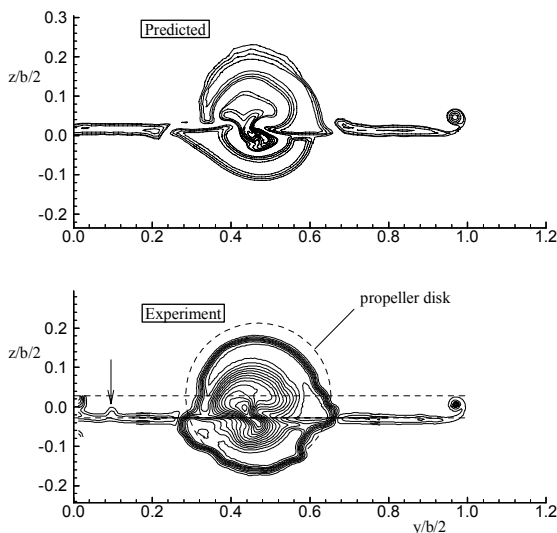


Fig. 32 Example of predicted and experimental contour lines of constant total pressure coefficient; prop on; $\alpha = 4^\circ$.

Table 3 Comparison of numerical and experimental (balance) data; RKE=Realizable $k-\epsilon$ model; RSM=Reynolds Stress model..

| | | propeller off | |
|-------|-----------------|--------------------|--------------------|
| | | $\alpha = 0^\circ$ | $\alpha = 4^\circ$ |
| C_D | Predicted (RKE) | 0.0169 | 0.0230 |
| | Predicted (RSM) | 0.0170 | 0.0231 |
| | Balance data | 0.0150 | 0.0198 |
| C_L | Predicted (RKE) | 0.000 | 0.291 |
| | Predicted (RSM) | 0.000 | 0.305 |
| | Balance data | 0.000 | 0.290 |

| | | propeller on | |
|-------|-----------------|--------------------|--------------------|
| | | $\alpha = 0^\circ$ | $\alpha = 4^\circ$ |
| C_D | Predicted (RKE) | -0.0929 | -0.0857 |
| | Predicted (RSM) | -0.0926 | -0.0842 |
| | Balance data | -0.0986 | -0.0916 |
| C_L | Predicted (RKE) | 0.004 | 0.316 |
| | Predicted (RSM) | 0.004 | 0.319 |
| | Balance data | 0.006 | 0.314 |

6 Conclusions

Experiments on propeller-wing configurations reveal a very complex flow with high levels of vorticity and considerable shearing forces in the wing area that is washed by the propeller slipstream.

Surface pressure measurements clearly showed the effect of the swirl velocity and the increased total pressure due to the propeller whose local influence is directly coupled to the propeller rotational direction. The force measurements and the surface pressure measurements demonstrated a performance benefit when the propeller rotational direction is inboard up. This finding indicates the possibilities to design optimum wing shapes whose exact shaping and profiling depends on the structure of the incoming slipstream.

With respect to the coupling between thrust and drag it seems that in many investigations the accuracy as well as the changes in the propeller thrust forces due to interference received limited attention. This approach is mostly reflected in ignoring the wing effect on the propeller (SIM). The full interaction mode (FIM) that used in the VLM calculations showed that even for a normal layout, with the tractor propeller well in front of the nacelle, small effects on the thrust coefficient are found in the range of several drag counts.

From the parametric study of the propeller position effects the following conclusions may be drawn.

- propeller inboard up rotation is beneficial as higher lift/drag ratios are obtained at constant power settings
- The effect of the propeller spanwise position is negligible for locations well within the range that is normally used for modern turboprop aircraft. Nevertheless, an inboard up rotating propeller positioned close to or at the wing tip delivers a considerable performance increase.
- When the vertical position of the propeller is changed, high positioned propellers obtain the highest lift coefficients. The drag coefficient, on the other hand, rises for both high and low propeller positions and shows a relative decrease for $z_p \approx 0$ due to the "donut" effect. It is important to notice that the calculations prove a low propeller position to be beneficial regarding the propulsive efficiency. The reason for this effect is attributed to the reduced propeller inflow distortion due to the wing.
- The streamwise variation of the propeller position shows small variations in the propulsive efficiency of the configuration. For positions further away from the wing ($x_p < 0$) the propulsive efficiency increases slightly due to the rise in the axial flow velocity inside the

slipstream and the diminished wing effect on the propeller.

- Negative propeller inclination angle with respect to the wing are in general beneficial for values of $\alpha_p < 15^\circ$. The main reason for this positive effect is the change in the slipstream velocity distribution where increased asymmetry is introduced and the fact that the complete slipstream envelope is rotated to produce an average increase in the local wing flow angle of attack.

The calculations performed with the different codes described herein in general conform to the trends found in the windtunnel experiments. The VLM-approach delivered quite accurate results compared to the panel methods and NS-code. This close agreement is found only after applying a swirl recovery factor (SRF). In the in the panel methods based on a slipstream envelope model that is solved simultaneously with the other parts of the numerical model, the absence of the SRF always leads to an overestimation the slipstream swirl velocity component and hence the local lift effect. In the inclusion method where the slipstream generated velocities and pressure are prescribed on a per-panel basis, SRF can be incorporated without difficulty. Hence this panel method approach is preferred over the slipstream envelope model.

Once accurate results are needed for the propeller-wing interference problem and details of the flow are needed to determine the secondary flow effects that influence the lift and drag performance of the model, the NS-code becomes indispensable.

The NS-approach facilitated the identification of typical flow phenomena, like the deformation of the slipstream when passing the wing. As indicated before, the spanwise distributions of lift and drag forces are sensitive to the form the velocity distribution in the slipstream as well as the way the slipstream deforms when passing the wing. Hence, a calculation model based on the NS-equation yields a more realistic estimation of the propeller wing interactive flow since the slipstream is allowed to develop and

deform freely and no artificial swirl recovery (the application of the SRF) is needed.

References

- [1] Miranda, L.R. and Brennan, J.E.: "Aerodynamic effects of wing tip mounted propellers and turbines", AIAA 86-1802, 1986, p. 221-228
- [2] Lötstedt, P.: "Accuracy of a propeller model in inviscid flow", Journal of Aircraft, vol. 32, No. 6, Nov./Dec. 1995
- [3] Lötstedt, P.: "A Propeller Slipstream Model in Subsonic Linearized Potential Flow", ICAS 90-5.4.4, 1990.
- [4] Aljabri, A.S.: "The prediction of propeller/wing interaction effects", ICAS 82-4.4.5, 1982.
- [5] Beek, C.M. van ; Piers, W.J. and Oskam, B. : "Aerodynamic analysis of slipstream/wing/nacelle interference for preliminary design of aircraft configurations", AGARD CP-498, 1991.
- [6] Katz, J. and Plotkin, A.: "Low speed aerodynamics – From wing theory to panel methods", ISBN 0-07-050446-6, Mc. Graw-Hill, 1991
- [7] Bertin, J.J.: "Aerodynamics for engineers", Prentice Hall, 4th edition, 2002, ISBN 0-13-064633
- [8] Anon.: "Fluent users manual, Version 6.1", Jan. 2003.
- [9] Veldhuis, L.L.M. and Nebiolo, S.: "A propeller-integration study comparing experimental data with numerical flow solutions based on the Navier-Stokes equations", ICAS 2000.
- [10] Nebiolo, S.: "CFD-analysis of a basic propeller-nacelle-wing configuration based on the solution of the Navier-Stokes equations", MSc. thesis, Delft University of Technology, 1999
- [11] Kroo, I , Propeller / wing integration for minimum induced loss, J. of Aircraft , July 1986, Vol. 23 , No. 7 , p. 561-565
- [12] Veldhuis, L.L.M. and Heyma, P.M.: "A Simple Wing Optimization Code Including Propeller Effects", ICAS 1998
- [13] Silverstein, A. and Wilson, H.A.: "Drag and propulsive characteristics of air-cooled engine-nacelle installations for large airplanes", NACA Report 746, 1939
- [14] Borne, P.C.M. and Hengst, J. van: "Investigation of propeller slipstream effects on the Fokker 50 through in-flight pressure measurements", AIAA-90-3084, 1990
- [15] Kuijvenhoven, J.L.: "Validation of propeller-slipstream calculations using a multi-block euler code", AIAA-90-3035, 1990
- [16] Ruhmaben: "Prediction of propeller slipstream-wing-nacelle aerodynamic interference using a higher order panel method", MSc. thesis, Delft University of Technology, 1994